Electronic Supplementary Information

Vapor Incubation of $FASnI_3$ films for Efficient and Stable Lead-free Inverted Perovskite Solar Cells

Ligang Xu[a,b], Chi Zhang[a], Xiangyun Feng[a], Wenxuan Lv[a], ZuQiang Huang[a], Wenzhen Lv[a], Chao Zheng[a], Guichuan Xing[c], Wei Huang[a,d] and Runfeng Chen[a]**

[a] *Key Laboratory for Organic Electronics and Information Displays & Jiangsu Key Laboratory for Biosensors, Institute of Advanced Materials (IAM), Nanjing University of Posts & Telecommunications, 9 Wenyuan Road, Nanjing 210023, China.*

[b] *Wuhan National Laboratory for Optoelectronics, Huazhong University of Science and Technology, Wuhan 430074, Hubei, China.*

[c] *Joint Key Laboratory of the Ministry of Education, Institute of Applied Physics and Materials Engineering, University of Macau, Avenida da Universidade, Taipa, Macau 999078, China.*

[d] *Frontiers Science Center for Flexible Electronics (FSCFE), Shaanxi Institute of Flexible Electronics (SIFE) & Shaanxi Institute of Biomedical Materials and Engineering (SIBME), Northwestern Polytechnical University (NPU), 127 West Youyi Road, Xi'an 710072, China.*

* Corresponding author. E-mail: iamrfchen@njupt.edu.cn; gcxing@um.edu.mo

1. Materials

Poly(3,4-ethylenedioxythiophene):poly(styrenesulfonate) (PEDOT:PSS) water dispersion was obtained from Heraeus (Clevios P VP.Al 4083). Formamidinium iodide (FAI) (≥ 99.5%) was purchased from Xi'an Polymer Light Technology Co., Ltd. Tin iodide (SnI_2, 99.99%) and tin fluoride (SnF_2, 99%) were from Sigma-Aldrich Co., Ltd and Aladdin, respectively. Fullerene (C_{60}) and bathocuproine (BCP, 99.7%) were obtained from Luminescence Technology Co., Ltd. Solvents of N,N-dimethylformamide (DMF, 99.5%), dimethyl sulfoxide (DMSO, > 99.9%), chlorobenzene (CB, 99.5%), and ethyl acetate (EA, >98%) were from either Acros Organics, Alfa Aesar, or TCL (Shanghai) Development Co., Ltd. MoO_3 and Al were purchased from Ji'lin OLED Co., Ltd and ZhongNuo Advanced Material (Beijing) Technology Co., Ltd, respectively. All these materials were used as received without further treatment.

2. Device fabrication and characterization

Indium tin oxide (ITO) electrode on glass substrate was cleaned in deionized (DI) water, acetone, and ethanol subsequently and respectively for 20 min in an ultrasonicator (Shumei KQ300DE). After dried with nitrogen gas, the ITO anode surface was treated with UV-ozone using a ODT UV-O_3 Cleaner for 15 min. Then, PEDOT:PSS solution was spin-coated on ITO at 4000 rpm for 60 s in air, followed by annealing at 120^{o}C for 20 min. The PEDOT:PSS-coated ITO was transferred into a glove box filled with high-purity N_2. The $FASnI_3$ precursor was prepared by mixing FAI, SnI_2 and SnF_2 at a molar ratio of 1:1:0.1 and a concentration of 1.0 mol/L in a mixed solvent of DMF/DMSO (4/1, v/v) and stirring at 60 ^{o}C for 2 h.

The conventional fabrication process of $FASnI_3$ films was carried out very similar to the literature reports. $FASnI_3$ precursor in the mixed solvent (1.0 mol/L) was spin-coated on the surface of ITO/PEDOT:PSS substrates at 5000 rpm for 30 s, then 150 μL of chlorobenzene was quickly dropped on the center of the substrates at the 13th s of the spin-coating process to produce the dense perovskite crystal film followed by 70°C thermal annealing for 10 min to remove residual solvents and promote further crystallization.

The novel "vapor incubation" (VI) treatment was performed as follows. Firstly, 3 mL ethyl acetate (EA) was dropped onto a blank glass substrate spinning at 1000 rpm for 5 min to promote the

vaporization of the EA and generate the vapor at the room temperature. During the spinning, the spin coater's chamber was open. The vapor concentration can be adjusted by the delay time between the pre-spinning with ethyl acetate and spinning of the perovskite precursor solution, considering that EA vapor will diffuse into the surrounding atmosphere for a decreased EA vapor concentration after its spinning and different EA vapor concentration will be obtained after different delay time. Thus, the weak-polar solvent vapor atmosphere of EA for VI was developed. At delay time around 2.0 h, the standard fabrication of perovskite crystal film was performed in this atmosphere with the identical procedures to the fabrication of conventional perovskite films.

The inverted perovskite solar cells (PSCs) were prepared by thermally depositing the electron transport layers of C_{60} (20 nm) and BCP (6 nm) and cathode of Al (100 nm) on the perovskite active layer in a vacuum chamber ($< 5\times10^{-4}$ Pa). C_{60} was deposited at a rate of 0.5 Å s^{-1} and the deposition rates of BCP and Al were 2 and 10 Å s^{-1}, respectively. The thicknesses of the layers, monitored by an oscillating quartz thickness monitor, were confirmed by a Bruker Dektak XT stylus profiler. The active area of the device was controlled to be 3×3 mm^2. Both the control PSCs prepared in standard normal procedures and VI-treated PSCs prepared in EA vapor were fabricated and investigated.

The fabricated devices were measured without encapsulation at room temperature (25°C) in N_2 atmosphere. Their photocurrent density-voltage (*J–V*) curves and power conversion efficiencies (PCEs) were obtained by a computer-programmed Keithley 2400 source/meter under 100 mW/cm^2 illumination of AM 1.5G solar simulator (SAN-EI Electric Co., Ltd.). The external quantum efficiency (EQE) measurements were conducted in air by QE-R system (Enli Technology Co., Ltd.). The hole-only devices with the structure of ITO/PEDOT:PSS (~ 40 nm)/perovskite (135 nm)/MoO_3 (10 nm)/Al (100 nm) were measured from 0 to 7 V with a step size of 0.02 V under dark conditions using the *J-V* sweep mode developed by a Keithley 2400 source/meter unit. For long-term photostability test, the unsealed devices were illuminated under continuous 100 mW cm^{-2} irradiation by a LED grow light (Spectrum King MLH140) in the glove box (H_2O < 1.0 ppm and O_2 <1.0 ppm).

Absorption spectra were obtained on a Jasco V-750 UV-Visible/Near Infrared Spectrophotometers. X−ray diffraction (XRD) and scanning electron microscopy (SEM) characterizations of $FASnI_3$ films were conducted on Rigaku Smart lab X-Ray diffractometer and Hitachi S-4800 scan electron microscope, respectively. Steady-state photoluminescence (PL) spectra were collected using Hitachi F-4600 spectrofluorometer (Japan). The time-resolved PL decays of the perovskite films on ITO substrates were measured by an Edinburgh FLS 980. A 485 nm pulse laser with a repetition frequency of ~1–20 MHz was employed. To identify the PL lifetime from the decay curve, we refer to the equation of $I=I_0A_1\times\exp[-(t/\tau_1)^{\beta}]+ I_0A_2\times\exp[-(t/\tau_2)^{\beta}]$, where I and I_0 are PL intensity and the initial PL intensity at time zero, τ is the lifetime and β is the stretching exponent ($0 < \beta < 1$). X-ray photoelectron spectroscopy (XPS) experiments were carried out on a ESCALAB 250 system equipped with a monochromatic Al Kα X-ray source (hv=1486.6 eV). The atomic force microscopy (AFM) measurements were performed at room temperature using Bruker Dimension Icon AFM equipped with Scanasyst-Air peak force tapping mode AFM tips from Bruker. The electrochemical impedance spectra (EIS) were measured on a CHI660 electrochemical workstation (CH Instrument Inc.). A 20 mV voltage perturbation was applied at different direct current voltages ranging from 0 to 0.4 V with frequencies between 10^5 and 1 Hz under dark conditions. The results were fitted using the software of Zsim. All characterizations and measurements were performed in ambient conditions.

The hole-only devices were fabricated with the structure of ITO/PEDOT:PSS (~ 20 nm)/perovskite (~ 135 nm)/MoO_3 (10 nm)/Al (100 nm) to investigate the trap density and mobility. J-V curves were measured from 0 to 7 V with a step size of 0.02 V under dark conditions using the *J-V* sweep mode on a Keithley 2400 source/meter unit. From the J-V curves, trap state density (n_{trap}) can be calculated by the following equation according to the space charge limit current:

$$n_{trap} = \frac{2\varepsilon\varepsilon_0 V_{TFL}}{qL^2}$$

where ε_0 is relative dielectric constant, ε is the vacuum dielectric constant, V_{TFL} is the trap filling limited (TFL) voltage, L is the film thickness. The ε_0 and L of $FASnI_3$ is ~25.0 and 135 nm, respectively. $\varepsilon=8.85\times10^{-12}$ F/m

The mobility (μ) was can be achieved by fitting the child region using by the Mott−Gurney law,

$$J = \frac{9}{8}\varepsilon_0 \varepsilon \mu \frac{V^2}{L^3}$$

where the V signify applied bias, respectively.

3. Supplementary Fig. parts

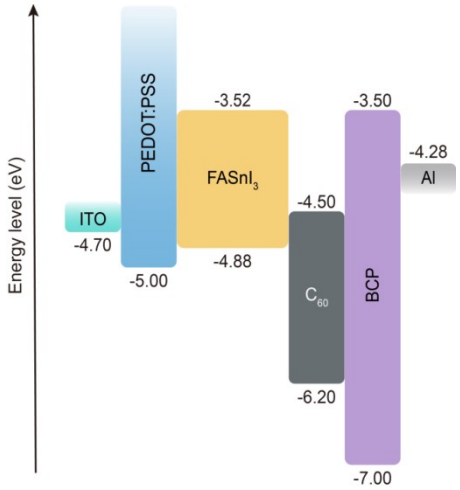

Fig. S1. Energy level diagram of the inverted lead-free Sn-based PSCs.

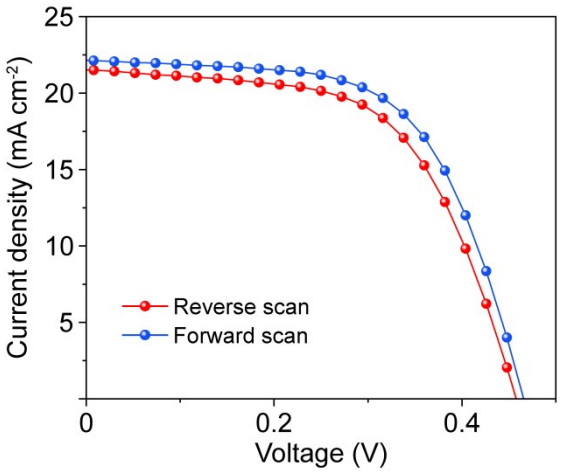

Fig. S2. J–V curves of the control PSC under reverse and forward scans

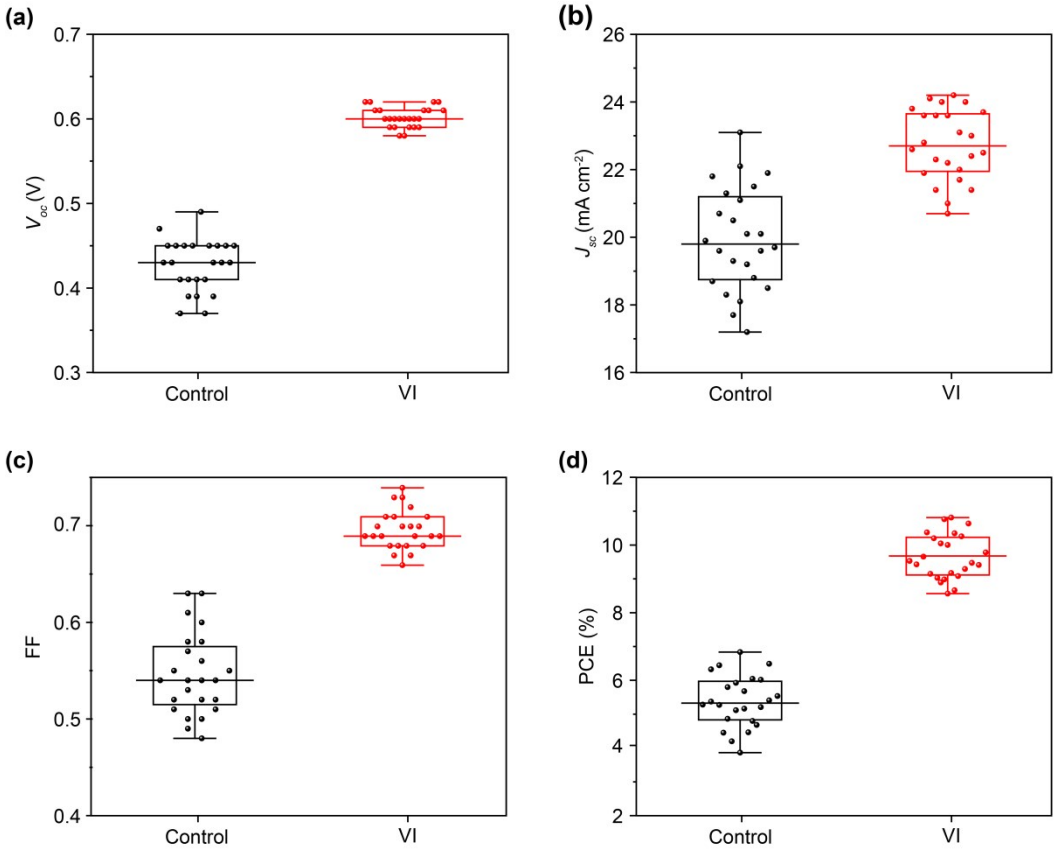

Fig. S3. Device performance statistics on (a) V_{oc}, (b) J_{sc}, (c) FF, and (d) PCE of the control and VI-derived PSCs. The box edges represent the standard deviations, the whiskers represent the maximum and minimum of the distributions, and the central horizontal line represents the median from 24 cells.

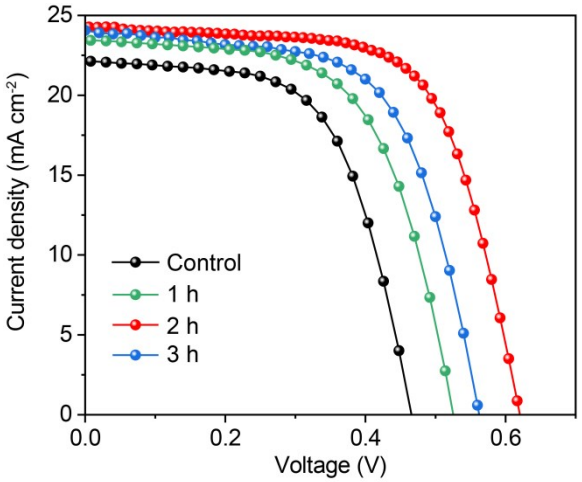

Fig. S4. J-V curves of the control and VI-derived devices with different delay time between the generation of EA vapor and spinning of the perovskite precursor solution.

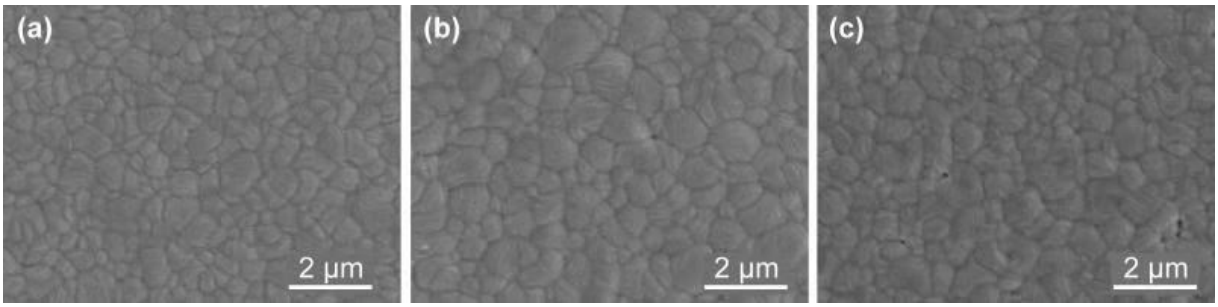

Fig. S5. SEM images of VI-treated $FASnI_3$ films with different delay time of (a) 1 h, (b) 2 h, and (c) 3 h between the generation of EA vapor and spinning of the perovskite precursor solution.

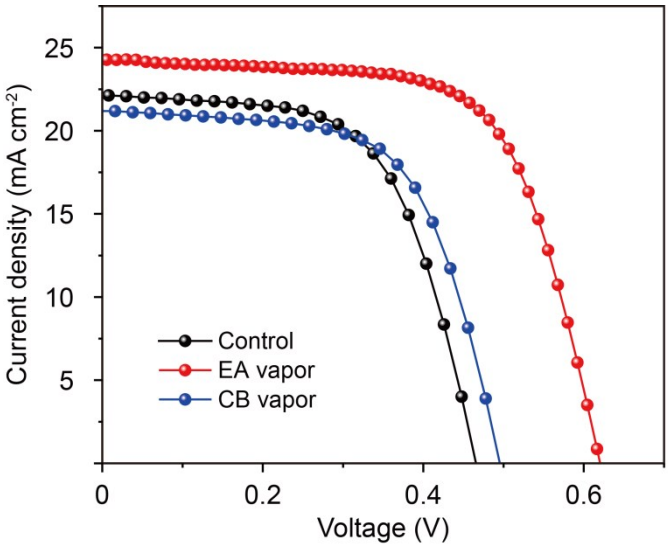

Fig. S6. J–V curves of the control and VI-derived devices treated using EA and CB vapor.

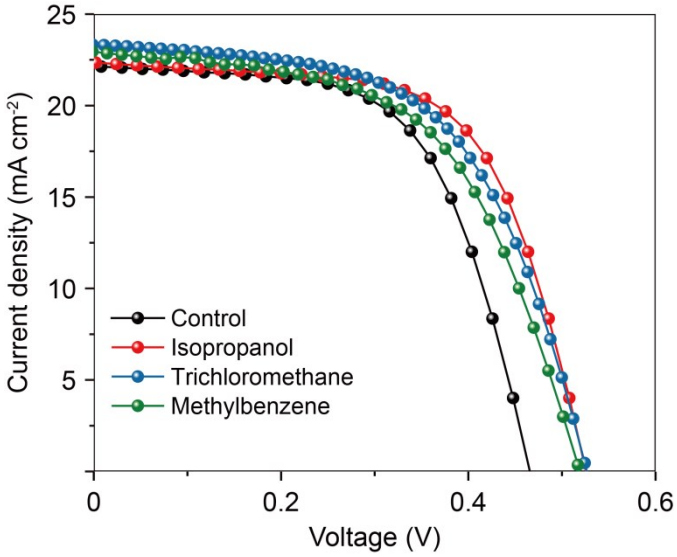

Fig. S7. J–V curves of VI -derived devices with different weak-polar solvent treatment.

.

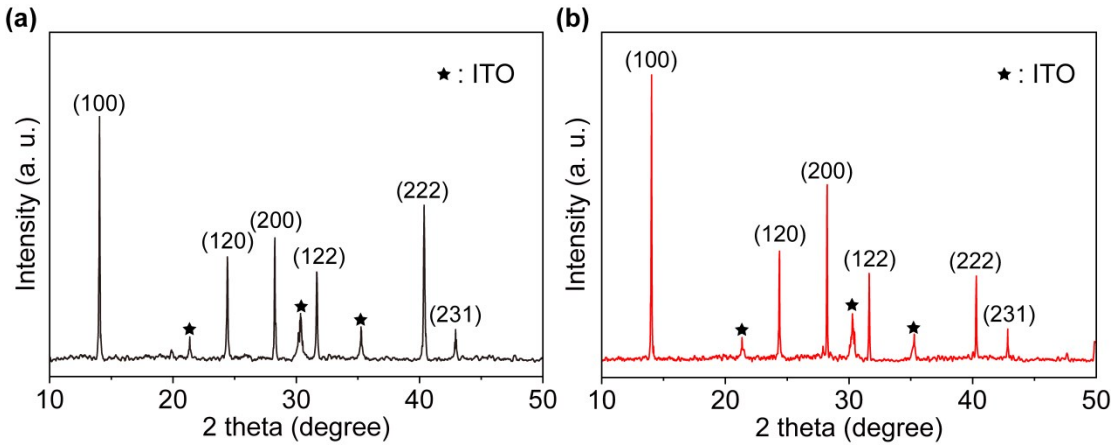

Fig. S8 XRD patterns of the VI-derived $FASnI_3$ films (a) before and (b) after chlorobenzene dripping and thermal annealing.

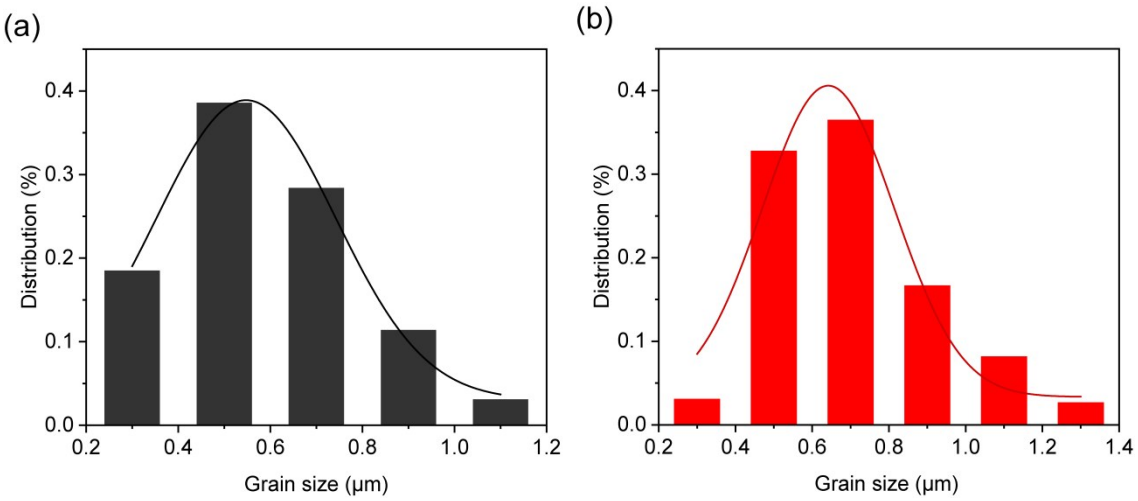

Fig. S9 Grain size distribution histograms of the perovskite particles in the (a) control and (b) VI - treated $FASnI_3$ films.

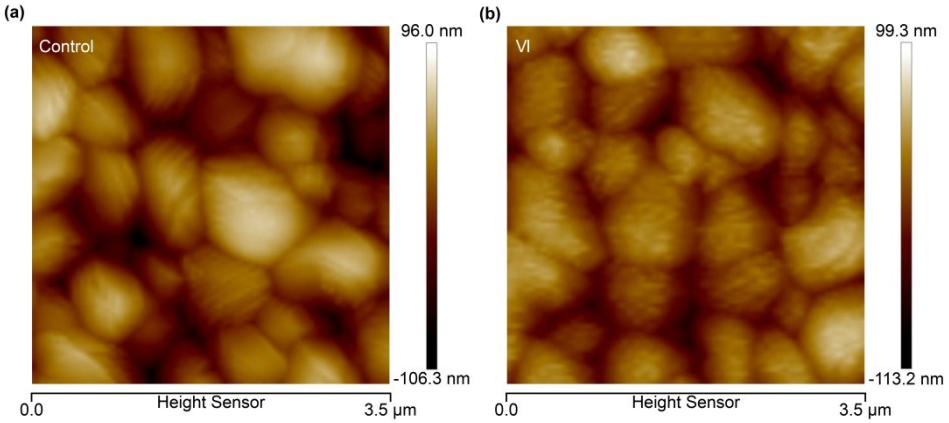

Fig. S10 AFM images of the (a) control and (b) VI -treated $FASnI_3$ perovskite films.

Fig. S11 $FASnI_3$ perovskite in EA solution (10 mg/mL).

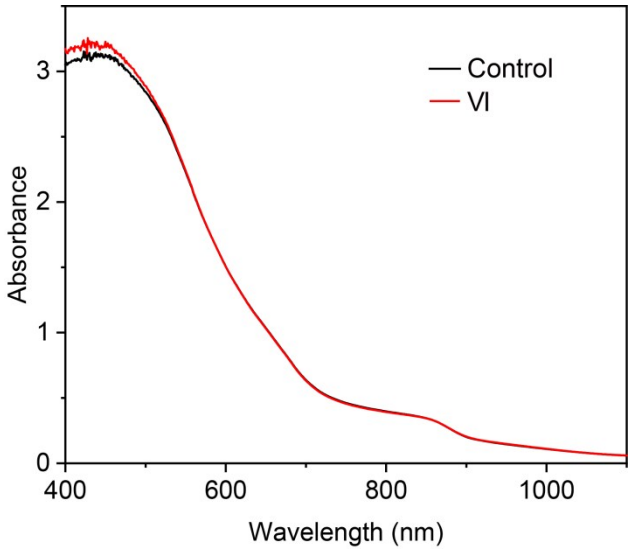

Fig. S12 Absorption spectra of the control and VI -treated $FASnI_3$ films.

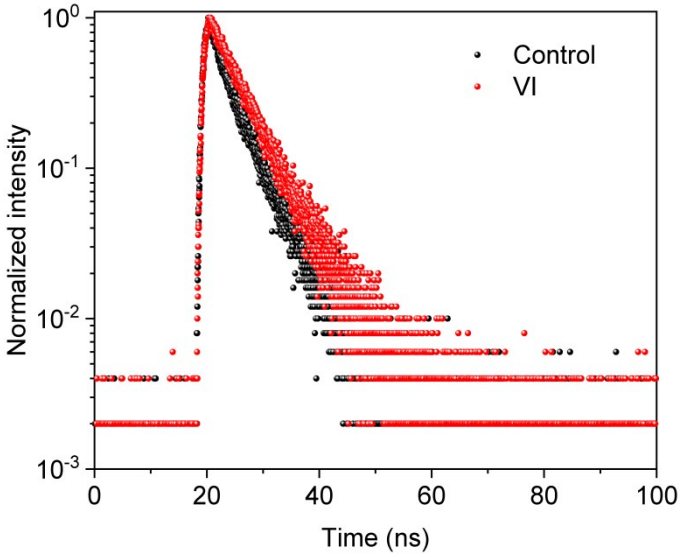

Fig. S13 TRPL spectra of the control and VI-treated $FASnI_3$ films

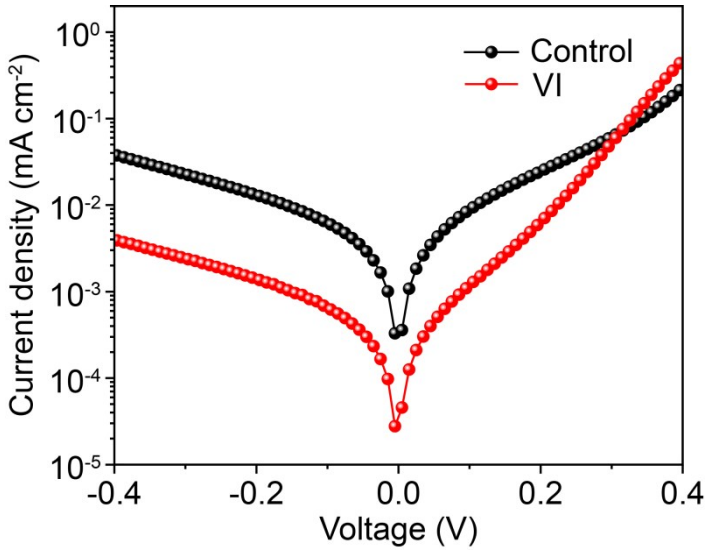

Fig. S14 Dark current characteristics of the control and VI -derived PSCs. The lower dark current density can be observed in the VI -derived PSC, suggesting that the current leakage is suppressed more effectively after the VI treatment.

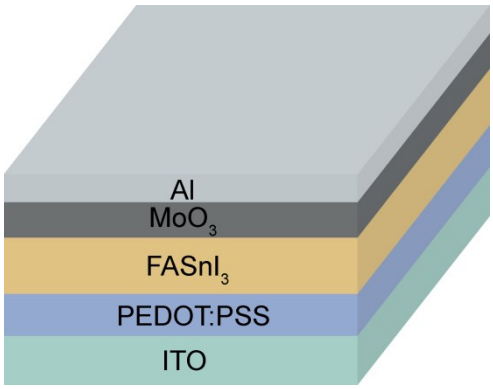

Fig. S15 Schematic structure of the hole-only device for the mobility and trap density measurements.

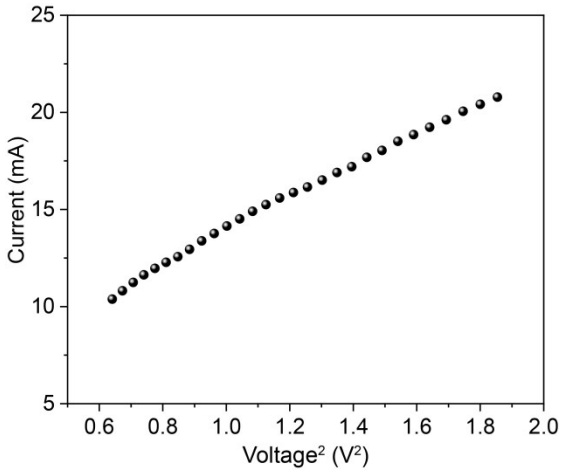

Fig. S16 J-V^2 curves of the child region of Fig. 3d

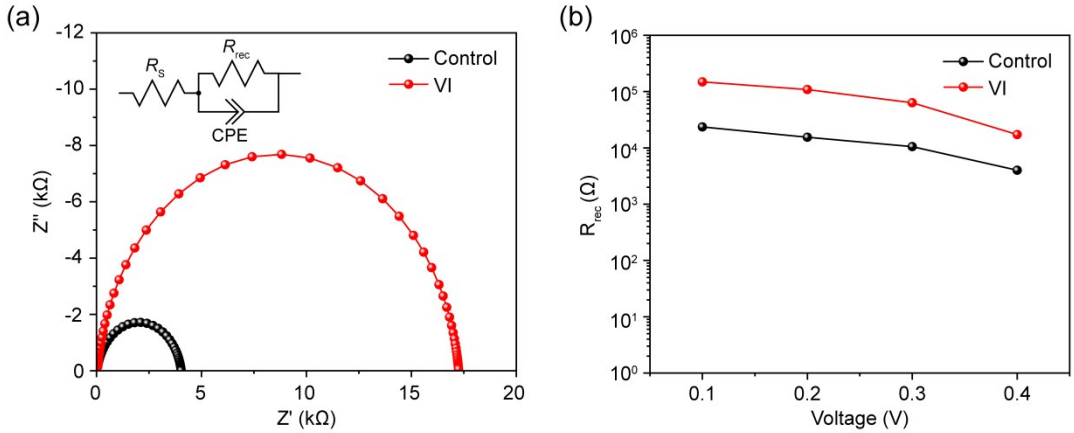

Fig. S17 (a) Nyquist plots of the EIS measurements of normal and VI -derived PSCs under dark condition, (b) Fitted R_{rec} at different applied voltages.

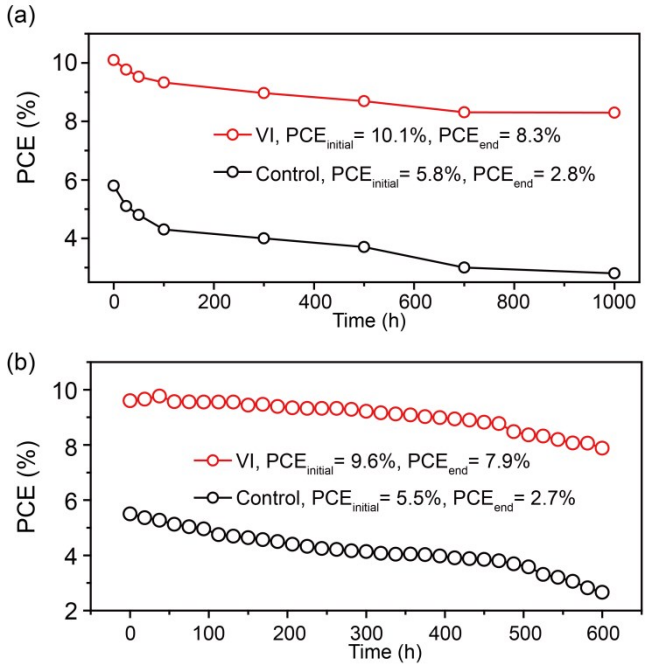

Fig. S18. Stability of the control and VI-derived $FASnI_3$ PSCs without encapsulation (a) stored in N_2 environment and (b) under one-sun illumination operating at MPPT. The $PCE_{initial}$ and PCE_{end} of devices were provided in the Figure.

Table S1. Performance data of the Sn-based PSCs reported in the literature.

Reference	V_{oc} [V]	J_{sc} [mA cm^{-2}]	FF	PCE [%]
Ref [1]	0.63	18.6	0.61	7.1
Ref [2]	0.62	21.2	0.73	9.6
Ref [3]	0.60	23.1	0.73	10.2
Ref [4]	0.94	17.4	0.75	12.4
Ref [5]	0.63	21.2	0.75	10.1
Ref [6]	0.61	22.0	0.70	9.4
Ref [7]	0.53	24.1	0.71	9.0
Ref [8]	0.59	18.9	0.62	7.0
Ref [9]	0.58	21.3	0.72	8.9
Ref [10]	0.56	23.3	0.74	9.6
Ref [11]	0.64	22.0	0.73	10.2
Ref [12]	0.63	20.4	0.69	8.9
Ref [13]	0.60	21.8	0.68	8.8
This work	0.62	24.2	0.72	10.8

Table S2. Device performance of Sn-based PSCs by varying the delay time between the generation of EA vapor and spinning of the perovskite precursor solution.

Time	V_{oc} [v]	J_{sc} [mA cm^{-2}]	FF	PCE [%]
1 h	0.52	23.4	0.62	7.6
2 h	0.62	24.2	0.72	10.8
3 h	0.56	24.0	0.63	8.5

Table S3. Device performance based on different antisolvents.

Antisolvent	V_{oc} [v]	J_{sc} [mA cm^{-2}]	FF	PCE [%]
CB	0.45	22.1	0.63	6.3
EA	0.34	12.5	0.49	2.9
CB+10 vt% EA	0.43	22.1	0.65	6.2

Table S4. Device performances under different annealing conditions

Condition	V_{oc} [v]	J_{sc} [mA cm^{-2}]	FF	PCE [%]
w/o EA vapor	0.45	22.1	0.63	6.3
With EA vapor	0.47	22.5	0.59	6.2

Table S5. The XPS fitting parameters of control and VI-treated $FASnI_3$ films.

Perovskite	peak position	KWHM	Area	Sn^{2+}/Sn^{4+} ratio
Control	486.4 (Sn^{2+}); 487.1 (Sn^{4+})	0.61 (Sn^{2+}); 0.70 (Sn^{4+})	49567 (Sn^{2+}); 26309 (Sn^{4+})	1.88
VI-treated	486.6 (Sn^{2+}); 487.2 (Sn^{2+})	0.60 (Sn^{2+}); 0.90(Sn^{4+})	58065 (Sn^{2+}); 17618 (Sn^{4+})	3.30

Table S6. The stability of the Sn-based PSCs reported in the literatures.

Perovskite	PCE (%)	Stability	Reference
$CsSnI_3$	3.56	25% RH, unencapsulated, continuous 1 sun irradiation, 16 h (70%)	14
$CsSnI_3$	4.30	40% RH, shelf stability, 100 h (98%)	15
$FASnI_3$	6.75	N_2, unencapsulated, 860 h (90%)	16
$FASnI_3$	5.4	N_2, 1000 h (65%)	17
$FASnI_3$	9.47	20% RH, encapsulated, MPPT, 600 h (93%)	18
$FASnI_3$	5.3	Continuous 1 sun irradiation, 350 h (60%)	19
$FASnI_3$	7.34	20% RH, shelf stability, unencapsulated, 500 h (50%)	20
$FASnI_3$	9.03	20% RH, shelf stability, unencapsulated, 1000 h (80%)	21
$FASnI_3$	11.5%	N_2, shelf stability, unencapsulated, 50 d (100%)	22
$FASnI_3$	11.39	In air, continuous 1 sun irradiation, 200 h (80%)	23
$FASnI_3$	10.8	N_2, unencapsulated, 1000 h (82%) or continuous 1 sun irradiation, 600 h (83%)	**This work**

Reference

[1] M. G. Ju, M. Chen, Y. Y. Zhou, J. Dai, L. Ma, N. P. Padture and X. C. Zeng, *Joule*, 2018, **2**, 1231-1241.

[2] E. Jokar, C. H. Chien, C. M. Tsai, A. Fathi and E. W. G. Diau, *Adv. Mater.*, 2019, **31**, 1804835.

[3] M. A. Kamarudin, D. Hirotani, Z. Wang, K. Hamada, K. Nishimura, Q. Shen, T. Toyoda, S. Iikubo, T. Minemoto, K. Yoshino and S. Hayase, *J. Phys. Chem. Lett.*, 2019, **10**, 5277-5283.

[4] X. Y. Jiang, F. Wang, Q. Wei, H. S. Li, Y. Q. Shang, W. J. Zhou, C. Wang, P. H. Cheng, Q. Chen, L. W. Chen and Z. J. Ning, *Nat. Commun.*, 2020, **11**, 1245.

[5] T. H. Wu, X. Liu, X. He, Y. B. Wang, X. Y. Meng, T. Noda, X. D. Yang and L. Y. Han, *Sci. China-Chem.*, 2020, **63**, 107-115.

[6] F. Wang, X. Y. Jiang, H. Chen, Y. Q. Shang, H. F. Liu, J. L. Wei, W. J. Zhou, H. L. He, W. M. Liu and Z. J. Ning, *Joule*, 2018, **2**, 2732-2743.

[7] S. Y. Shao, J. Liu, G. Portale, H. H. Fang, G. R. Blake, G. H. ten Brink, L. J. A. Koster and M. A. Loi, *Adv. Energy Mater.*, 2018, **8**, 1702019.

[8] M. E. Kayesh, K. Matsuishi, R. Kaneko, S. Kazaoui, J. J. Lee, T. Noda and A. Islam, *ACS Energy Lett.*, 2019, **4**, 278-284.

[9] E. Jokar, C. H. Chien, A. Fathi, M. Rameez, Y. H. Chang, E. W. G. Diau, *Energy Environ. Sci.*, 2018, **11**, 2353-2362.

[10] C. X. Ran, W. Y. Gao, J. R. Li, J. Xi, L. Li, J. F. Dai, Y. G. Yang, X. Y. Gao, H. Dong, B. Jiao, I. Spanopoulos, C. D. Malliakas, X. Hou and M. G. Kanatzidis, Z. X. Wu, *Joule*, 2019, **3**, 3072-3087.

[11] X. Y. Meng, Y. B. Wang, J. B. Lin, X. Liu, X. He, J. Barbaud, T. H. Wu, T. Noda, X. D. Yang, L. Y. Han, Surface-Controlled Oriented Growth of $FASnI_3$ Crystals for Efficient Lead-free Perovskite Solar Cells. *Joule*, 2020, **4**, 902-912.

[12] X. Y. Meng, Y. B. Wang, J. B. Lin, X. Liu, X. He, J. Barbaud, T. H. Wu, T. Noda, X. D. Yang and L. Y. Han, *Joule*, 2020, **4**, 902-912.

[13] J. Qiu, Y. D. Xia, Y. T. Zheng, W. Hui, H. Gu, W. B. Yuan, H. Yu, L. F. Chao, T. T. Niu, Y. G. Yang, X. Y. Gao, Y. H. Chen and W. Huang, *ACS Energy Lett.*, 2019, **4**, 1513-1520.

[14] K. P. Marshall, M. Walker, R. I. Walton and R. A. Hatton, *Nat. Energy*, 2016, **1**, 16178.

[15] J. H. Heo, J. Kim, H. Kim, S. H. Moon, S. H. Im and K. H. Hong, *J. Phys. Chem. Lett.*, 2018, **9**, 6024–6031.

[16] F. Gu, S. Ye, Z. Zhao, H. Rao, Z. Liu, Z. Bian and C. Huang, *Sol. RRL*, 2018, **2**, 1800136.

[17] M. E. Kayesh, T. H. Chowdhury, K. Matsuishi, R. Kaneko, S. Kazaoui, J. J. Lee, T. Noda and A. Islam, *ACS Energy Lett.*, 2018, 1584–1589.

[18] X. He, T. Wu, X. Liu, Y. Wang, X. Meng, J. Wu, T. Noda, X. Yang, Y. Moritomo, H. Segawa and L. Han, *J. Mater. Chem. A*, 2020, **8**, 2760–2768.

[19] B. B. Yu, L. Xu, M. Liao, Y. Wu, F. Liu, Z. He, J. Ding, W. Chen, B. Tu, Y. Lin, Y. Zhu, X. Zhang, W. Yao, A. B. Djurisic, J. S. Hu and Z. He, *Sol. RRL*, 2019, **3**, 1800290.

[20] J. Cao, Q. Tai, P. You, G. Tang, T. Wang, N. Wang and F. Yan, *J. Mater. Chem. A*, 2019, **7**, 26580–26585.

[21] T. Wang, Q. Tai, X. Guo, J. Cao, C. K. Liu, N. Wang, D. Shen, Y. Zhu, C. S. Lee and F. Yan, *ACS Energy Lett.*, 2020, **5**, 1741–1749.

[22] T. Nakamura, S. Yakumaru, M. A. Truong, K. Kim, J. Liu,S. Hu, K. Otsuka, R. Hashimoto, R. Murdey, T. Sasamori, H. D. Kim, H. Ohkita, T. Handa, Y. Kanemitsu and A. Wakamiya, *Nat. Commun.*, 2020, **11**, 3008.

[23] X. Meng, Y. Li, Y. Qu, H. Chen, N. Jiang, M. Li, D.-J. Xue, J.-S. Hu, H. Huang and S. Yang, *Angew. Chem. Int. Edit.*, 2021, **60**, 3693.